Materials and methods

Brain tissues were obtained from nine subjects (average age, 60.6 years; five men and four women) who had a neuropathologically confirmed diagnosis of MSA, and from five control subjects (average age, 62.2 years; one man and four women) who died of cancer, stroke, pneumonia, or myocardial infarction with no signs of neurodegeneration. Five-micrometer-thick sections of formalin-fixed, paraffin-embedded tissues from the pons were immunostained with the appropriate antibodies using the streptavidin–biotin method (Histofine SAB-PO kit; Nichirei, Tokyo, Japan). For all stainings, sections were deparaffinized and subsequently immersed in 0.3% hydrogen peroxide (H_2O_2) (Dojin Laboratories, Kumamoto, Japan) in methanol for 30 min, to block endogenous peroxidase activity. All sections were autoclaved for 10 min in 10 mM sodium citrate buffer (pH 6.0) for antigen retrieval. Immunoreactivity was visualized using 0.5 mg/ml of 3,3′-diaminobenzidine tetrachloride and 0.03% H_2O_2 (Dojin Laboratories). All sections were counterstained with hematoxylin. The specimens were observed under an Olympus DP72 microscope (Olympus, Tokyo, Japan) using the DP2-BSW software (Olympus, Tokyo, Japan).

In this study, we used the following commercially available antibodies: anti-lysosomal-associated membrane protein 1 (LAMP1; rabbit polyclonal; Abgent, San Diego, California, USA) [14], anti-lysosomal-associated membrane protein 2 (LAMP2; mouse monoclonal; Santa Cruz Biotechnology, Santa Cruz, California, USA) [15,16], anti-cathepsin D (rabbit polyclonal; Biogenex Laboratories, San Ramon, California, USA) [14], and anti-hexosaminidase subunit A (HEXA; rabbit polyclonal; Abgent, San Diego, California, USA) [17]. For statistical analysis, we calculated LAMP1-positive and cathepsin D-positive areas using Image-Pro Plus version 5.1 (Media Cybernetics, Bethesda, Maryland, USA). The sum of the areas from three pictures of each case was analyzed statistically using a *t*-test.

To assess the colocalization of lysosomal proteins with GCI-associated proteins, we performed double immunohistochemistry using fluorescent secondary antibodies [18]. The primary antibodies used for double immunohistochemistry were anti-α-synuclein (mouse monoclonal; Invitrogen, Carlsbad, California, USA) [19], anti-ubiquitin (mouse monoclonal; Chemicon International, Temecula, California, USA) [18], and anti-CD68 (mouse monoclonal; Dako Cytomation, Glostrup, Denmark). After deparaffinization and autoclaving, sections were incubated with the antibodies overnight at 4°C. The secondary antibody combinations used were Alexa Fluor 488 goat anti-mouse IgG (H + L; Molecular Probes-Invitrogen, Eugene, Oregon, USA) and Alexa Fluor 568 goat anti-rabbit IgG (H + L; Molecular Probes-Invitrogen). To avoid autofluorescence signals, sections were treated with Sudan Black B (Wako Pure Chemical Industries, Osaka, Japan) for 5 min and rinsed in 70% ethanol. Specimens were mounted with Vectashield (Vector Laboratories, Burlingame, California, USA) and examined under a microscope equipped with a confocal system (FV1000; Olympus, Tokyo, Japan). The images obtained were processed further using Adobe Photoshop CS4 Extended (Adobe, San Jose, California, USA).

Results

Lysosomes are acidic, membrane-bound organelles that are rich in hydrolases. For the evaluation of lysosomal pathology, we first used antibodies against lysosomal membrane proteins (LAMP1 and LAMP2) and lysosomal hydrolases (cathepsin D and HEXA) to analyze the pontocerebellar fibers of both normal controls and patients with neuropathologically proven MSA. In the control brains, the immunostaining profiles were characterized by cytoplasmic granules that might be considered to be lysosomes (Figs 1a, c, e, and g and 3a). Immunoreactivity for lysosomal markers in MSA brains was easily distinguishable from that of age-matched controls. A robust increase in LAMP1, LAMP2, cathepsin D, and HEXA staining in pontocerebellar fibers was observed in MSA brains (Fig. 1b, d, f, and h). The intensity of the staining in MSA brains was much stronger than that in control brains and the immunoreactivity area was extensive in the cytoplasm of many cells (Fig. 1). We assessed the immunoreactivity by measuring the positive area of staining for lysosomal markers. This analysis showed the presence of a significant increase in immunoreactivity in MSA compared with control samples (Fig. 2). In addition, we observed differences in the distribution and the number of lysosomal-protein-positive structures. In control brains,

Fig. 2

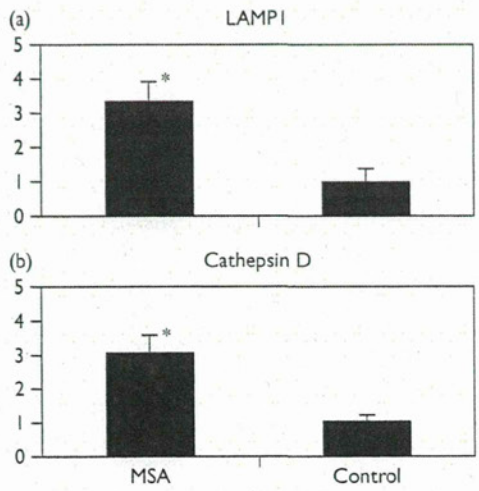

Statistical analysis of the immunopositive area for LAMP1 (a) and cathepsin D (b). Student's *t*-test revealed a significant difference of median values between control and MSA brains. *$P<0.01$ compared with control brains. LAMP1, anti-lysosomal-associated membrane protein 1; MSA, multiple system atrophy.

Fig. 3

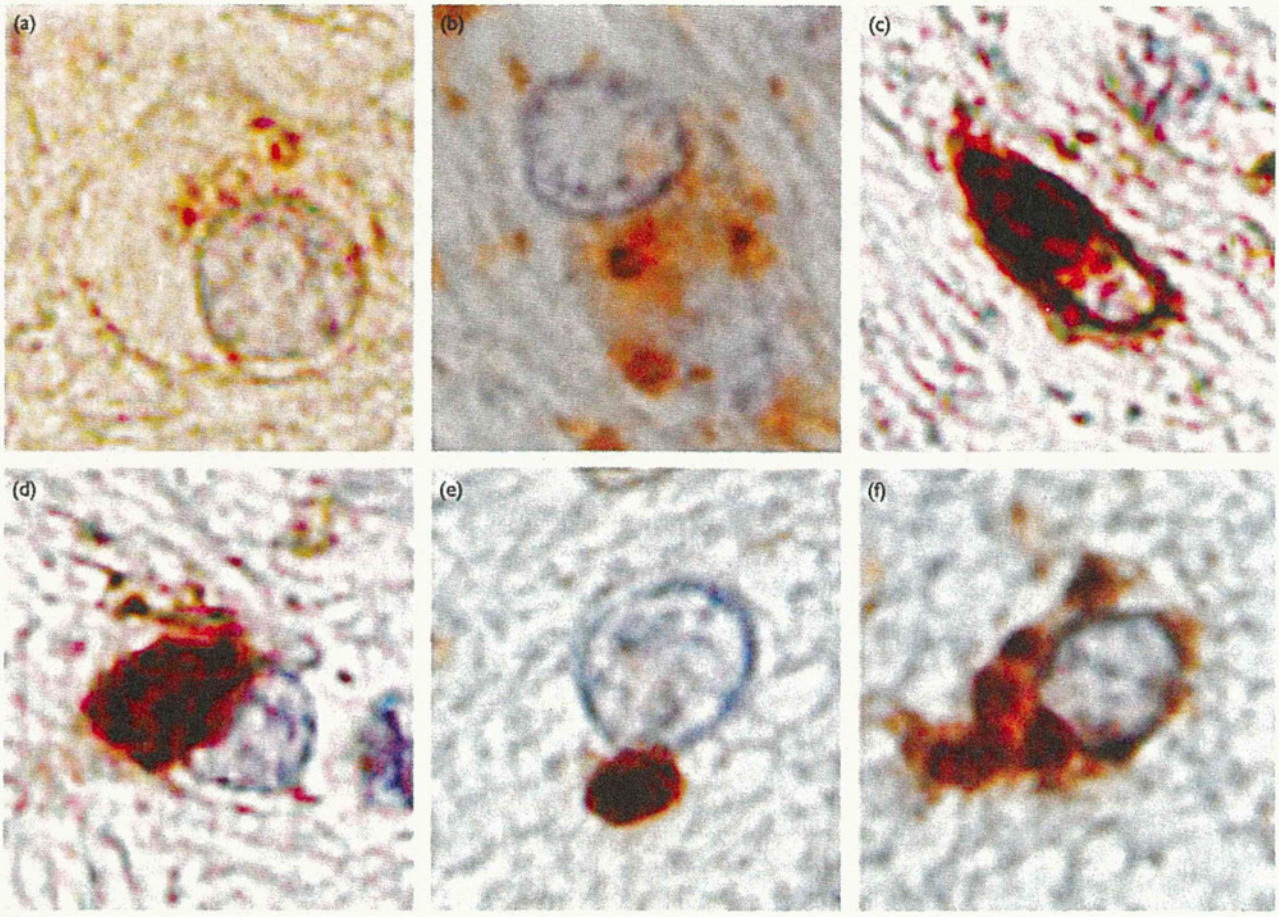

Immunohistochemical detection of the anti-LAMP1 antibody in control brains (a) and MSA brains (b–f). In the control brains, the immunostaining profiles were characterized by cytoplasmic granules (a). LAMP1-positive structures in MSA brains exhibited varying morphologies (b–f). LAMP1, anti-lysosomal-associated membrane protein 1; MSA, multiple system atrophy.

lysosomal-protein-positive structures were located around nuclei, with a few structures per cell (Figs 1a, c, e, and g and 3a). In contrast, lysosomal-protein-positive structures were distributed throughout the cytoplasm, and not only around nuclei, in MSA brains (Fig. 1b, d, f, and h). Furthermore, LAMP1-positive structures in MSA brains exhibited varying morphology. Some LAMP1-positive structures were dot-like, similar to those of controls, whereas the intensity of the staining was much stronger, and the size of structures was larger in comparison with controls (Fig. 3b). Furthermore, some cells were diffusely positive for LAMP1 in the cytoplasm (Fig. 3c), whereas others exhibited large inclusions in the majority of the cytoplasm (Fig. 3d). However, in a small number of samples, some cells had an oval structure or many round structures (Fig. 3e and f). In contrast, flame-shaped and sickle-shaped cytoplasmic structures, which were observed clearly as GCIs in the specimens stained with anti-α-synuclein antibodies in MSA brains, were not stained by anti-LAMP1 antibodies.

To determine whether alterations in lysosomal markers were associated with aberrant accumulation of α-synuclein, we performed confocal microscopy in MSA brains using dual staining for α-synuclein and each lysosomal marker. Most cells were extensively positive for lysosomal markers, but were rarely labeled for α-synuclein (Fig. 4a–f, arrows). Occasionally, the immunoreactivity of lysosomal markers was close to the immunoreactivity of α-synuclein-positive inclusions (Fig. 4a–f, arrowheads), but lysosomal-protein-positive structures in α-synuclein-positive cells were rare. Colocalization studies were carried out to evaluate whether ubiquitin, which is another GCI marker, was associated with altered expression of lysosomal markers. Similar to α-synuclein, ubiquitin rarely colocalized with lysosomal proteins in cells that were extensively positive for lysosomal proteins (Fig. 4g–i). To explain why lysosomal markers did not colocalize mainly with GCI-associated proteins, we considered that lysosomal alteration resulted from cells other than oligodendroglia. It has been reported that microglia are activated in MSA brains and that

Fig. 4

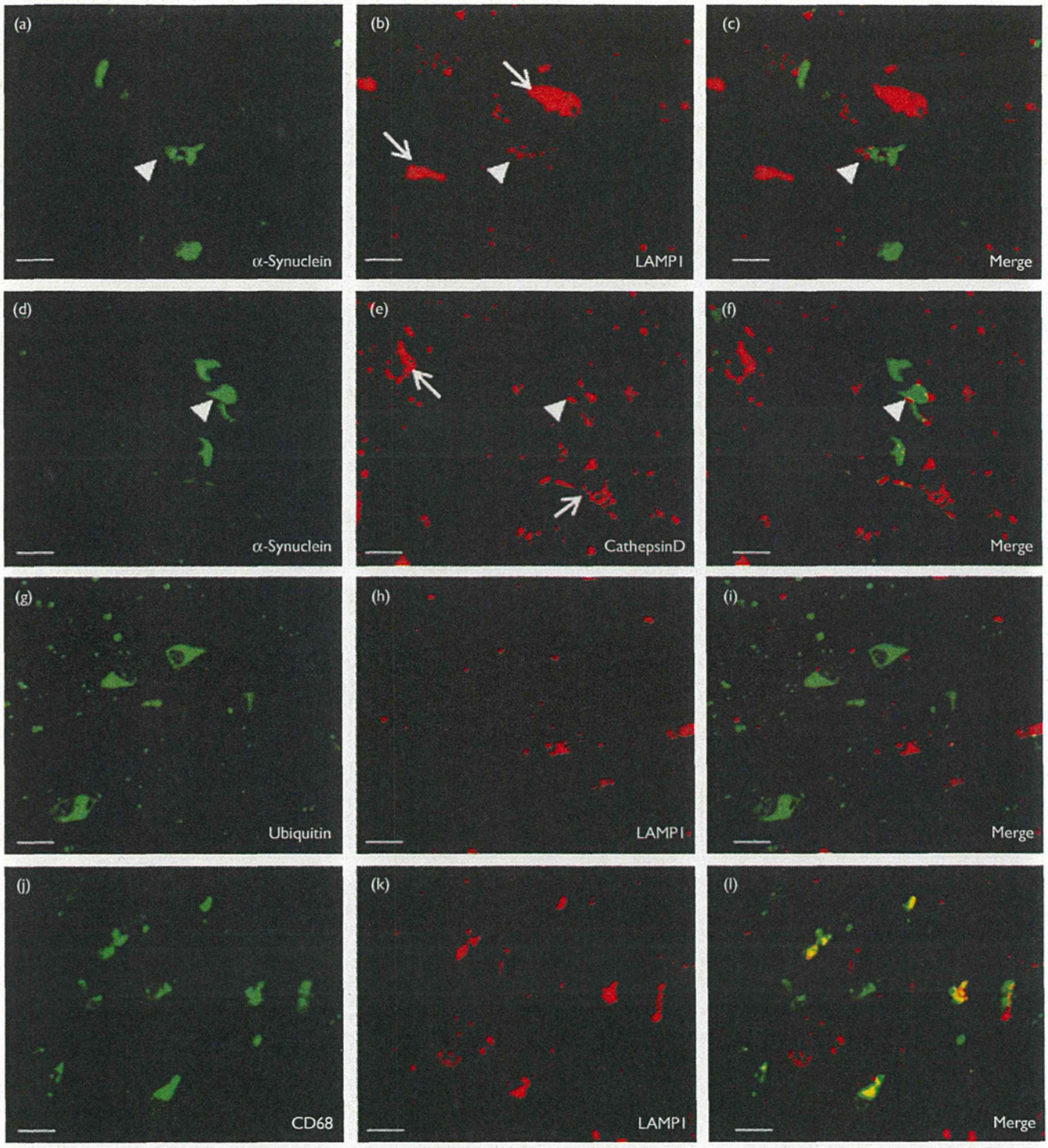

Double immunohistochemistry for α-synuclein (green) and lysosomal markers (LAMP1 and cathepsin D; red; a–f). Most cells were extensively positive for lysosomal markers, but were labeled rarely for α-synuclein (a–f, arrows). The immunoreactivity of lysosomal markers was occasionally close to α-synuclein-positive inclusions (a–f, arrowheads). Double immunohistochemistry for ubiquitin (green) and LAMP1 (red). Ubiquitin rarely colocalized with LAMP1 (g–i). Double immunohistochemistry for CD68 (green) and LAMP1 (red; j–l). CD68 colocalized with LAMP1 (j–l). Scale bar, 20 μm. LAMP1, anti-lysosomal-associated membrane protein 1; MSA, multiple system atrophy.

microglial activation mediates oligodendroglial α-synucleinopathy [20,21]. Therefore, we performed confocal microscopy using dual staining for LAMP1 and CD68, which are microglial markers, and found that many LAMP1-positive cells were positive for CD68 (Fig. 4j–l).

Discussion

In this study, we demonstrated that immunoreactivity for lysosomal proteins was increased in MSA brains. This indicates that lysosomes are activated in MSA brains. Moreover, we observed lysosomal alterations regarding the morphology, the number, and the distribution of lysosomes in the cytoplasm of MSA brains compared with lysosomes observed in control brains. Thus, lysosomal alterations in MSA may indicate not only lysosomal activation but also lysosomal dysfunction. Lysosomes are cytoplasmic membrane-enclosed organelles that contain hydrolytic enzymes [5]. The high content of hydrolytic enzymes in lysosomes renders them harmful to cells. If the lysosomal membrane is damaged, lysosomes release their contents into the cytosol. Massive lysosomal breakdown may induce cytosolic acidification, which in turn can induce cell death by necrosis [22]. These lysosomal alterations in MSA brains may be related to the cell death and neurodegeneration observed in MSA.

There is increasing evidence that lysosomes are involved in the pathogenesis of a variety of neurodegenerative diseases, including AD and PD [17,23]. Immunoreactivity for lysosomal proteins is increased in AD brains, and alterations of the lysosomal system develop in pyramidal neurons in the neocortex and hippocampus before overt degenerative changes are apparent [24]. Moreover, lysosomal enzymes exist in senile plaques, which are one of the pathological hallmarks of AD [17]. These data indicate that lysosomal activation and alteration of lysosomes are induced by aberrant protein accumulation, and that lysosomes may play some role in the neurodegeneration associated with AD. In contrast, in PD (which is one of the α-synucleinopathies), immunoreactivity for lysosomal proteins is significantly decreased in nigral neurons that contain α-synuclein inclusions [12]. In our study, immunoreactivity for lysosomal proteins was increased in MSA brains, but lysosomal proteins colocalized rarely with α-synuclein-positive cells. Recently, it was reported that α-synuclein is degraded through the autophagy–lysosomal pathway [10,11]. Moreover, expression of mutant α-synuclein in neurons leads to lysosomal dysfunction [6,25]. Therefore, accumulation of α-synuclein in MSA brains does not induce lysosomal activation in cells that accumulate α-synuclein and may result in additional α-synuclein accumulation. Incompleteness of lysosomal systems in α-synucleinopathies may play a role in the accumulation of α-synuclein and in neurodegeneration.

Our double immunohistochemistry results revealed that the lysosomal-protein-positive structures localized mainly in cells that showed immunoreactivity for CD68, which is a microglial marker. The pathological features of MSA brain included the presence of GCIs in oligodendroglia. Conversely, it has been reported that microglia are activated and that microglial activation parallels system degeneration in MSA [20]. Moreover, phagocytosis of degenerating myelin by activating microglia has been observed in MSA brain [20]. These findings indicate that lysosomal activation and alteration in microglia play important roles in the pathogenesis of MSA. During the degenerative process of MSA, microglia are activated and may attempt to digest degenerating components, including myelin, through the endosome–lysosome pathway.

In summary, we demonstrated the presence of lysosomal activation and alteration in MSA brains. Lysosomal proteins colocalized rarely with α-synuclein, and immunoreactivity for lysosomal proteins was observed mainly in microglia. Although α-synuclein does not induce lysosomal activation directly, lysosomes in microglia are activated and altered during the process of neurodegeneration.

Acknowledgements

This study was supported by grants from the Ministry of Health, Labor, and Welfare and the Ministry of Education, Culture, Sports, Science, and Technology of Japan to K. Okamoto.

Conflicts of interest

There are no conflicts of interest.

References

1 Soto C. Unfolding the role of protein misfolding in neurodegenerative diseases. *Nat Rev Neurosci* 2003; **4**:49–60.
2 Selkoe DJ, Schenk D. Alzheimer's disease: molecular understanding predicts amyloid-based therapeutics. *Annu Rev Pharmacol Toxicol* 2003; **43**:545–584.
3 Spillantini MG, Schmidt ML, Lee VM, Trojanowski JQ, Jakes R, Goedert M. α-Synuclein in Lewy bodies. *Nature* 1997; **388**:839–840.
4 Ciechanover A. Proteolysis: from the lysosome to ubiquitin and the proteasome. *Nat Rev* 2005; **6**:79–86.
5 Bellettato CM, Scarpa M. Pathophysiology of neuropathic lysosomal storage disorders. *J Inherit Metab Dis* 2010; **33**:347–362.
6 Bahr BA, Bendiske J. The neuropathogenic contributions of lysosomal dysfunction. *J Neurochem* 2002; **83**:481–489.
7 Papp MI, Kahn JE, Lantos PL. Glial cytoplasmic inclusions in the CNS of patients with multiple system atrophy (striatonigral degeneration, olivopontocerebellar atrophy and Shy–Drager syndrome). *J Neurol Sci* 1989; **94**:79–100.
8 Arima K, Ueda K, Sunohara N, Arakawa K, Hirai S, Nakamura M, *et al.* NACP/α-synuclein immunoreactivity in fibrillary components of neuronal and oligodendroglial cytoplasmic inclusions in the pontine nuclei in multiple system atrophy. *Acta Neuropathol* 1998; **96**:439–444.
9 Bennett MC, Bishop JF, Leng Y, Chock PB, Chase TN, Mouradian MM. Degradation of α-synuclein by proteasome. *J Biol Chem* 1999; **274**:33855–33858.
10 Mak SK, McCormack AL, Manning-Bog AB, Cuervo AM, Di Monte DA. Lysosomal degradation of alpha-synuclein *in vivo*. *J Biol Chem* 2010; **285**:13621–13629.
11 Xilouri M, Vogiatzi T, Vekrellis K, Stefanis L. α-Synuclein degradation by autophagic pathways: a potential key to Parkinson's disease pathogenesis. *Autophagy* 2008; **4**:917–919.
12 Chu Y, Dodiya H, Aebischer P, Olanow CW, Kordower JH. Alterations in lysosomal and proteasomal markers in Parkinson's disease: relationship to α-synuclein inclusions. *Neurobiol Dis* 2009; **3**:385–398.

13 Jellinger KA, Lantos PL. Papp–Lantos inclusions and the pathogenesis of multiple system atrophy: an update. *Acta Neuropathol* 2010; **119**:657–667.
14 Funk KE, Mrak RE, Kuret J. Granulovacuolar degeneration (GVD) bodies of Alzheimer's disease (AD) resemble late-stage autophagic organelles. *Neuropathol Appl Neurobiol* 2011; **37**:295–306.
15 Higashi S, Moore DJ, Yamamoto R, Minegishi M, Sato K, Togo T, *et al.* Abnormal localization of leucine-rich repeat kinase 2 to the endosomal–lysosomal compartment in Lewy body disease. *J Neuropathol Exp Neurol* 2009; **68**:994–1005.
16 Higashi S, Moore DJ, Minegishi M, Kasanuki K, Fujishiro H, Kabuta T, *et al.* Localization of MAP1-LC3 in vulnerable neurons and Lewy bodies in brains of patients with dementia with Lewy bodies. *J Neuropathol Exp Neurol* 2011; **70**:264–280.
17 Cataldo AM, Paskevich PA, Kominami E, Nixon RA. Lysosomal hydrolases of different classes are abnormally distributed in brains of patients with Alzheimer disease. *Proc Natl Acad Sci USA* 1991; **88**:10998–11002.
18 Kadokura A, Yamazaki T, Kakuda S, Makioka K, Lemere CA, Fujita Y, *et al.* Phosphorylation-dependent TDP-43 antibody detects intraneuronal dot-like structures showing morphological characters of granulovacuolar degeneration. *Neurosci Lett* 2009; **463**:87–92.
19 Oh D, Prayson RA. Evaluation of epithelial and keratin markers in glioblastoma multiforme: an immunohistochemical study. *Arch Pathol Lab Med* 1999; **123**:917–920.
20 Ishizawa K, Komori T, Sasaki S, Arai N, Mizutani T, Hirose T. Microglial activation parallels system degeneration in multiple system atrophy. *J Neuropathol Exp Neurol* 2004; **63**:43–52.
21 Stefanova N, Reindl M, Neumann M, Kahle PJ, Poewe W, Wenning GK. Microglial activation mediates neurodegeneration related to oligodendroglial α-synucleinopathy: implications for multiple system atrophy. *Mov Disord* 2007; **22**:2196–2203.
22 Boya P, Kroemer G. Lysosomal membrane permeabilization in cell death. *Oncogene* 2008; **27**:6434–6451.
23 Zhang L, Sheng R, Qin Z. The lysosome and neurodegenerative diseases. *Acta Biochim Biophys Sin* 2009; **41**:437–445.
24 Nixon RA, Cataldo AM, Paskevich PA, Hamilton DJ, Wheelock TR, Kanaley-Andrews L. The lysosomal system in neurons. Involvement at multiple stages of Alzheimer's disease pathogenesis. *Ann NY Acad Sci* 1992; **674**:65–88.
25 Stefanis L, Larsen KE, Rideout HJ, Sulzer D, Greene LA. Expression of A53T mutant but not wild-type α-synuclein in PC12 cells induces alterations of the ubiquitin-dependent degradation system, loss of dopamine release, and autophagic cell death. *J Neurosci* 2001; **21**:9549–9560.

INTERNAL MEDICINE

□ CASE REPORT □

A Novel GJA1 Mutation in Oculodentodigital Dysplasia with Progressive Spastic Paraplegia and Sensory Deficits

Natsumi Furuta[1,3], Masaki Ikeda[1], Kimitoshi Hirayanagi[1,3], Yukio Fujita[1], Makoto Amanuma[2] and Koichi Okamoto[1]

Abstract

Oculodentodigital dysplasia (ODDD) is a rare autosomal dominant inherited disorder mainly affecting the development of the face, eyes, dentition, limbs, hair and heart. *GJA1* (the gap junction protein α-1) has been determined to be a causative gene of ODDD, mapped to chromosome 6q22-24 identified as the connexin 43 gene (Cx43). We found a novel *GJA1* mutation (W25C) as the possible causative gene in this sporadic ODDD patient with neurological features of motor deficits by pyramidal tract signs, and sensory deficits due to peripheral nerve disturbance. It is also notable that the MRI of this patient demonstrated widespread aberrant signal lesions in the brain and brainstem.

Key words: oculodentodigital dysplasia (ODDD), GJA1, mutation, spastic paraparesis, peripheral sensory nerve deficits, MRI

(Intern Med 51: 93-98, 2012)
(DOI: 10.2169/internalmedicine.51.5770)

Introduction

Oculodentodigital dysplasia (ODDD, OMIM 164200) is a rare autosomal dominant inherited disorder affecting the development of face, teeth, limbs, hair and heart. Affected individuals have a long, narrow nose with hypoplastic alae and a prominent nasal bridge, short palpebral fissures and bilateral microcornea, often with iris anomalies (1, 2). The characteristic digital abnormality is bilateral complete syndactyly of the fourth and fifth fingers (type III syndactyly); the third finger may also be involved (1). Additionally, microdontia and enamel hypoplasia, which tend to affect both the primary and secondary dentitions, are often observed (1, 3). Neurological symptoms observed in ODDD include dysarthria, neurogenic bladder disturbances, spastic paraparesis, ataxia, anterior tibial muscle weakness and seizures (4). Mild mental retardation occurs infrequently. In some cases, MRI studies of patients with ODDD have shown diffuse bilateral abnormalities in the subcortical cerebral white matter, which can define a slowly progressive leukodystrophy (4). Paznekas et al identified missense mutations of ODDD patients in the Cx43 gene, that is, the gap junction protein α-1 gene (*GJA1*), in all 17 studied families with ODDD (5). ODDD is usually inherited as an autosomal dominant trait with high penetrance (4), although autosomal recessive inheritance, sporadic cases have also been documented in some ODDD cases (4, 6, 7). These findings have been confirmed and extended by a series of studies that demonstrate clearly that the pleiotropic features observed in ODDD bearing missense mutations of *GJA1* (8-13). Here, we report a sporadic ODDD patient with a novel *GJA1* mutation, who presented with weakness and spasticity, along with sensory deficits that are rare manifestations. With regard to the sensory symptoms, we confirmed abnormal findings of peripheral sensory nerves by nerve conduction study.

Case Report

The patient, a 34-year-old-woman, had a congenital specific facial appearance including microgenia, hypoplastic alae nasi, internal epicanthus, tooth enamel dysplasia and syndactyly of the hands. Because of increasing unsteadiness of gait over the three years and the numbness of bilateral

[1]Department of Neurology, Gunma University Graduate School of Medicine, Japan, [2]Diagnostic Radiology and Nuclear Medicine, Gunma University Graduate School of Medicine, Japan and [3]Department of Neurology, Maebashi Red Cross Hospital, Japan
Received for publication May 6, 2011; Accepted for publication September 15, 2011
Correspondence to Dr. Masaki Ikeda, mikeda@med.gunma-u.ac.jp

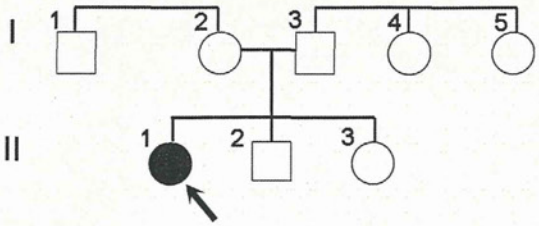

Figure 1. Pedigree of this family. Two-generation pedigree of an ODDD family. The proband is indicated by an arrow. There are no signs of the clinical abnormalities of ODDD in members of her family. Her parents (68-year-old father, 65-year-old mother) are clinically normal, and not related in any way. Circles indicate female family members and squares indicates male family members.

foot bottoms, she was referred to our hospital for further investigation from another hospital. She is the second child of non-consanguineous healthy parents; she has an elder sister and a younger brother. Her father (68 years old), mother (65 years old) and other relatives have no such symptoms as this proband (Fig. 1). Growth and mental development were normal. She had surgery for bilateral syndactyly of fingers IV-V at 1 year old. Ocular anomalies comprised microcornea, microphthalmos and developmental glaucoma. She had lost her right visual field. At age 22, she had trabeculectomy because her left intraocular pressure was not controlled. Then she was clinically diagnosed with ODDD because of her specific facial appearance and other physical abnormalities. At age 31, she began to feel unsteadiness of gait and stiffness of the legs. During the past year, she reported episodes of falling. At age 34, because of increasing unsteadiness of gait, she was admitted to our hospital. She had a spastic tetraparesis with hyperreflexia, a pronounced scissor gait, and limb hyperreflexia. Foot clonus and patellar clonus were present. She complained of numbness of bilateral foot bottoms. In her clinical history, she had not suffered from diabetes mellitus, spinal cord or vertebral diseases, or collagen diseases presenting peripheral neuropathies. Cranial nerves and autonomic nervous systems were normal. Deep senses of toe position and vibration were intact. General examination revealed bilateral blepharoptosis, short, scarce eyelashes, converged strabismus, epicanthus and blepharoptosis of both eyes, and micrognathia (small chin), with curly, soft and very fine hairs (Fig. 2A). Her teeth were abnormal with different degrees of enamel hypoplasia and taurodontism (Fig. 2B). She had bilateral camptodactyly of fingers IV and V, and clinodactyly of finger V, with scars of hand surgery (Fig. 2C) as also shown in X-P (Fig. 2D).

The laboratory data of serum and cerebrospinal fluid was normal. Nerve conduction studies were undertaken. Motor conduction velocity and the amplitudes of median, ulnar, peroneal and tibial nerves were normal. Sensory conduction velocity of bilateral median, ulnar, and sural nerves was delayed as well as the amplitude was low and distal latency was delayed. Sensory conduction velocity of the sural nerve was not detected at all (Table 1).

Brain MRI showed low signal changes in the bilateral globus pallidus internal segment (GPi) on T1- and T2-weighted images (T1WI, T2WI) (Fig. 3A, B, C). Abnormal high signal on T2WI was observed in the bilateral posterior limbs of internal capsula, corona radiata and centrum semiovale (Fig. 3A, D, E). Brain CT revealed bilateral dense calcification of the GPi (Fig. 3F). In midbrain on T2WI MRI, bilateral cerebral peduncle showed high signals (Fig. 3G:→). An abnormal high signal of transverse fibers (→) and longitudinal fibers (→) was observed in the mid-pons (Fig. 3H), as well as a high signal of transverse fibers (→) and longitudinal fibers (→) was observed in the lower pons (Fig. 3I). Aberrant high signal changes in the internal capsula, cerebral peduncle in the midbrain and in the ventral side of the pons corresponded to the corticospinal tract, that is, the pyramidal tract.

After obtaining informed consent for this genetic test approval by the Ethics Committees in Gunma University, we determined mutation analysis. We purified genomic DNA from lymphocytes in the peripheral blood of the proband. Purified genomic DNA was sequenced according to a previous method (14, 15). One microgram of genomic DNA isolated from leukocytes was mixed with 0.5 μg of each primer, followed by amplification through 30 cycles under the following conditions: 94℃ for 30 s for denaturation, 60 ℃ for 30 s for annealing, and 72℃ for 30 s for elongation.

The GJA1 coding exon was amplified in two overlapping fragments using the primers 5′-AAT ACG TGA AAC CGT TGG TAG-3′ and 5′-CTC TTT CCC TTA ACC CGA TC-3′, which amplified a product of 856 bp, and 5′-TCT TTG AGG TGG CCT TCT TG-3′ and 5′-TAA GGC TGT TGA GTA CCA CC-3′, which amplified a product of 773 bp (16). The PCR product was excised from 2.5% Nusieve (FMC Bioproducts, Rockland, ME) agarose gel, purified, and treated with T vector cloning system pGEM-T® (PROMEGA). Then, the plasmid clones were subjected to sequencing using an ABI 3130XL genetic analyzer DNA sequencer (Applied Biosystems, Foster City, CA, USA) as specified by the manufacturer. The sequence result revealed that heterozygous with "TGG" for normal allele and "TGT" for mutant allele, namely, W (tryptophan) to C (cysteine) at the third base of codon 25 (W25C) in the *GJA1* gene (Fig. 4). No similar mutation was observed in 100 normal alleles of 50 subjects providing informed consent. Unfortunately, we could not examine the same mutation in *GJA1* gene for her parents and siblings because they refused the genetic test. W25 is conserved between ten species from human to mycobacteria (human, bovine, dog, rat, mouse, chicken, zebrafish, drosophila, saccharomyces and mycobacteria). In the present patient's recent physical and neurological examinations, no particular change was observed. Her gait is still instable, but she is somehow able to walk by herself.

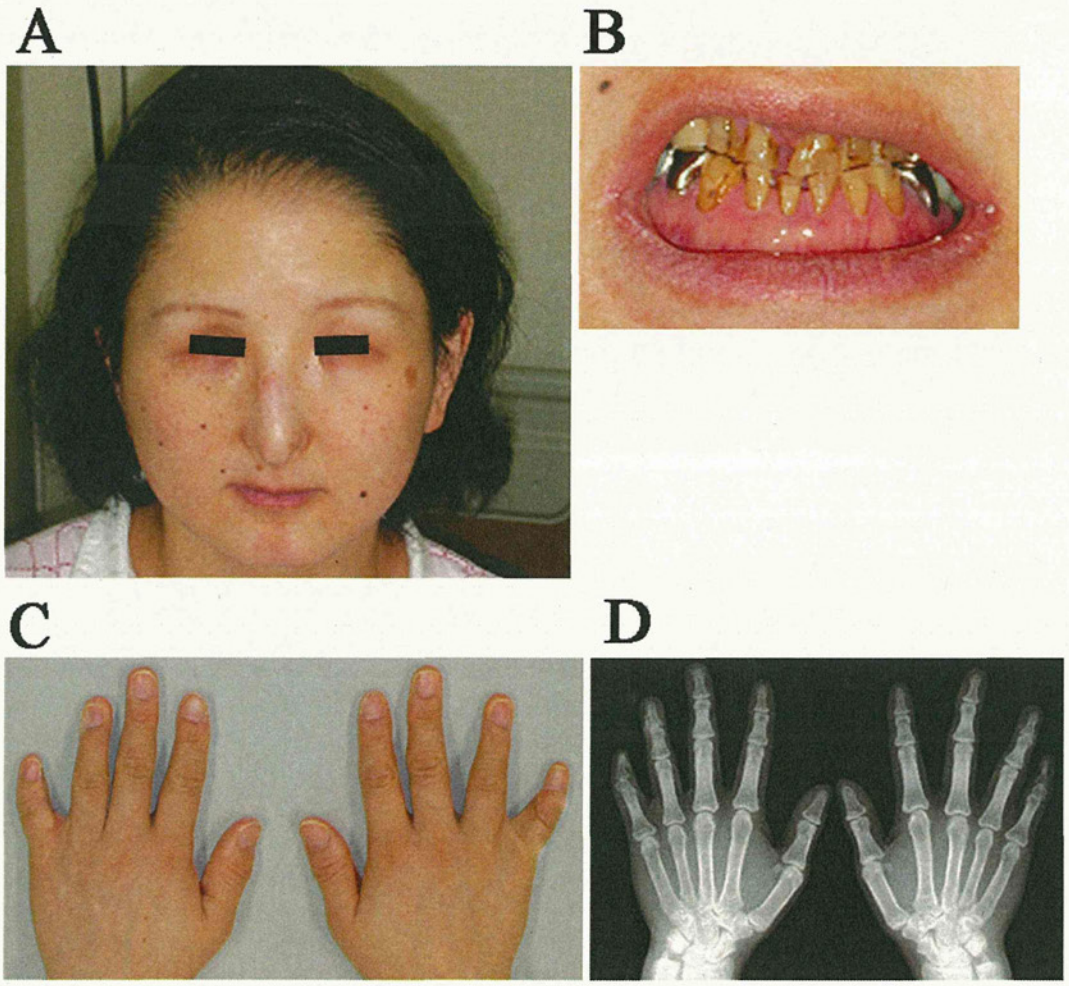

Figure 2. Appearance of this case. (A) This patient showed a thin and tapered nose, hypoplastic alae nasi, epicanthal folds and ocular asymmetry. Her hair was very thin and curly. (B) Her teeth were abnormal with enamel hypoplasia of a brown color and an irregular size for each tooth. (C) She had bilateral camptodactyly of fingers IV and V, and clinodactyly V. (D) X-ray showed clinodactyly of bilateral fingers V after operation.

Table 1. Nerve Conduction Examination

Name(Nerve)	R/L	MCV/SCV	Proxi. (ms)	Distal lat. (ms)	Distance (mm)	Velocity (m/s)	Amp. (Distal)
Median	R	MCV	5.92	2.82	180	58.1	18.65
Median	L	MCV	5.66	2.54	170	54.5	13.66
Ulnar	R	MCV	6.36	2.28	190	46.6	8.73
Ulnar	L	MCV	5.72	1.98	170	45.5	4.21
Peroneal	R	MCV	8.94	4.48	245	54.9	4.22
Peroneal	L	MCV	8.02	3.12	250	51	2.19
Tibial	R	MCV	10.94	3.74	340	47.2	10.53
Tibial	L	MCV	9.54	3.06	330	50.9	19.18
Median	R	SCV	9.1	n.d.	250	31.8	0.093
Median	L	SCV	7.14	n.d.	220	37.7	0.139
Ulnar	R	SCV	9.84	4.32	200	36.2	0.051
Ulnar	L	SCV	7.78	3.74	190	47	0.19
Sural	R	SCV	n.d.	n.d.	n.d.	n.d.	n.d.
Sural	L	SCV	n.d.	n.d.	n.d.	n.d.	n.d.

Nerve conduction examination revealed normal results in motor conduction velocity and amplitude of median, ulnar and peroneal nerves. sensory conduction velocity of bilateral median, ulnar, the tibial nerves was delayed, while the amplitude was low and distal latency was delayed. Sensory conduction velocity of the sural nerve was not detected.

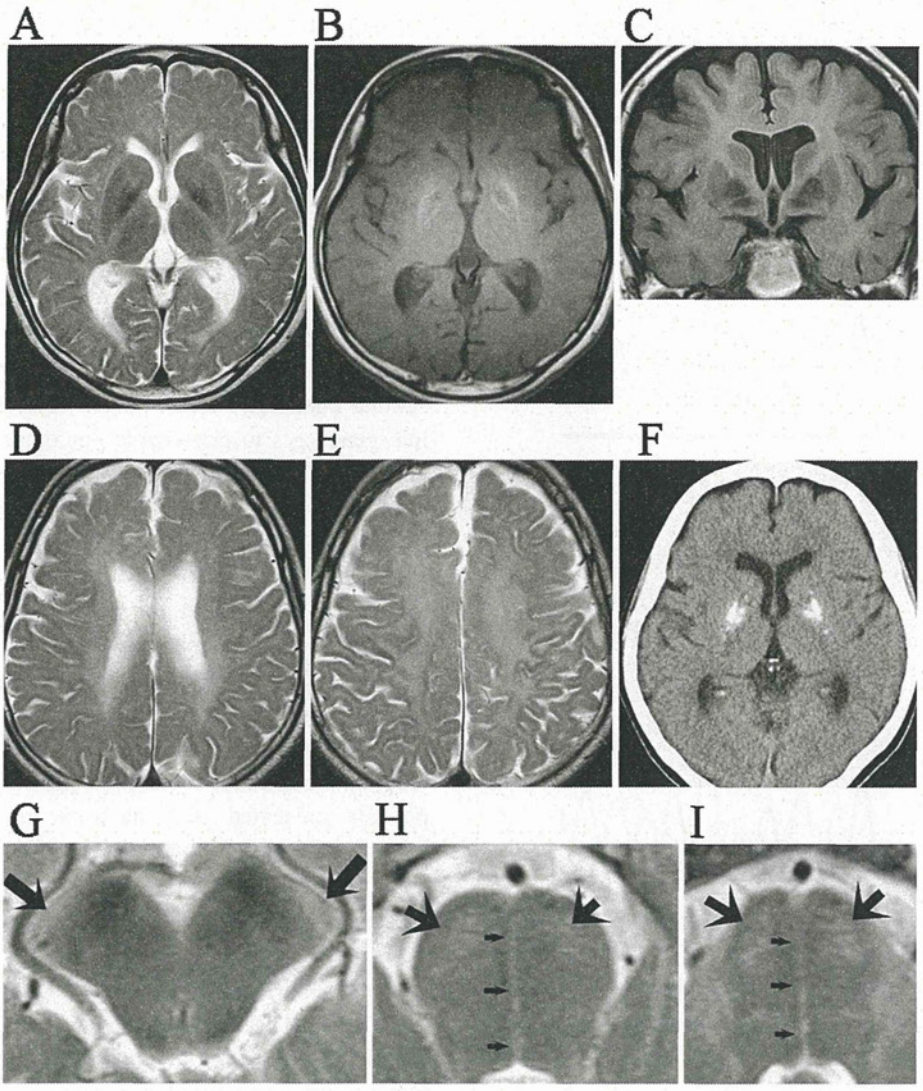

Figure 3. **MRI study. Aberrant low signal was observed in the bilateral globus pallidus internal segment (GPi) on T1WI and T2WI MRI (A, B, C). High signal was observed in the bilateral posterior limbs of internal capsula, corona radiata and centrum semiovale on T2WI (A, D, E). Bilateral calcification of the GPi was observed on CT scan (F). In midbrain, bilateral cerebral peduncle showed high signals on T2WI (G: ➡). Abnormal high signal of transverse fibers (➔) and longitudinal fibers (⟶) was observed in the mid-pons on T2WI (H), with the same findings as in bilateral corticospinal tracts of the lower pons on T2WI (I). A, D, E, G, H, I: T2WI (TR 4000/TE 86), B, C: T1WI (TR 518/TE 12).**

Discussion

Since Paznekas et al has found causative missense mutations in *GJA1* (5), more than 50 different mutations have been described (13). GJA1 or Cx43, like other connexin proteins, consists of an intracellular N-terminus, four transmembrane domains, two extracellular loops, one cytoplasmic loop and an intracellular C-terminus (5). Six connexins can form a connexon, a specialized intracellular structure surrounding a pore (17). Two connexons in apposing cell membranes can align to form an intercellular gap junction. These channels provide a direct low-resistance intercellular pathway for the passage of ions and small molecules that confer distinct physiological properties. Gap junctions have been found in the majority of mammalian tissues. Most tissues express more than one type of connexin, and multiple types of connexins can assemble to form gap junctions between cells, with the diversity of combinations influencing the nature of the cell-to-cell communication (18-20). In more than 240 reported cases of ODDD, most of these substitutions in *GJA1* have been located in the second intracellular and first transmembrane domains (13). Indeed, our novel *GJA1* mutation W25C is located in the first transmembrane domains. Among affected individuals, sensory deficits are very rare. Previous reports describe one patient with pain in the lower limbs (21), three patients with paresthesia (22, 23) and one patient with decreased vibration sensation in L90V muta-

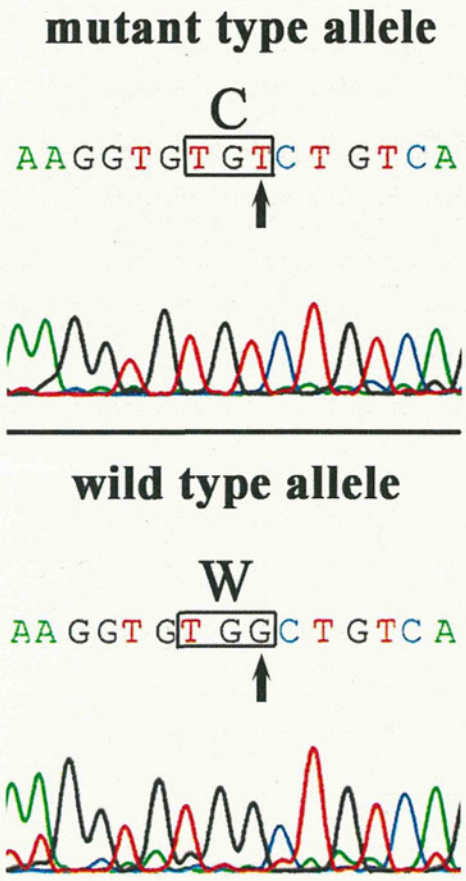

Figure 4. **Molecular analysis. Sequences of the PCR product spanning codon 25 of genomic *GJA1* DNA. The patient was heterozygous with "TGT" for normal allele and "TGG" for mutant allele, namely, to W (tryptophan) to C (cysteine) at the first base of codon 25 in the *GJA1*.**

tion (13). For the first time, we have confirmed sensory deficits by nerve conduction studies. Sensory conduction velocity of bilateral median, ulnar, and tibial nerves was delayed and the amplitude was low with distal latency. Sensory conduction velocity of the sural nerve was not detected. In her neurological examination, it is interesting that she showed both pyramidal tract signs (hyperreflexia and clonus) and sensory disturbance of the lower limbs, because wide spread neurodegeneration as an aberrant high signal change of pyramidal tract in brain and brainstem, and also peripheral sensory neuropathy might occur in both. We described clinical phenotypes of ocular, dentition, and digital due to developmental disorders, in addition to peripheral nerve disturbances and aberrant MRI findings of brain and brainstem, which are characteristic of this case as ODDD. Although there are some cases of aberrant MRI findings, we demonstrated novel evidences in which peripheral nerve disturbances were confirmed by electrical examination in an ODDD case.

Physiologically, Cx43 is expressed in the peripheral nerves, Schwann cells as well as other Cx family members of Cx26, 32, 37, 40, 45 and 46 (24). Mutant Cx43 may play aberrant roles in peripheral nerves and Schwann cells among gap junctions, resulting in demyelination. MRI of some Cx32 mutation patients (CMT-X: X-linked Charcot-Marie-Tooth disease) was reported to show diffuse high signal lesions in cerebral white matter (25, 27) as well as peripheral neuropathies. The disruption of gap junction communication between oligodendrocytes and astrocytes may involve the cellular mechanism by which GJB1 (Cx32) mutations cause a "CNS phenotype" (25).

In this inter-relationship between the same family proteins (connexins), mutant connexin Cx43 might have a trans-dominant effect to Cx32 due to functional changes of intercellular channels, Laird reported that Cx26 and Cx43 might link genotypes to phenotypic outcomes by aberration of gap junctions (26). To date, in some reported cases of ODDD, abnormal white matter high signal lesions on T2WI in nine cases were particularly marked in the periventricular parieto-occipital region and in the temporal lobe extending to the midfrontal region and the posterior limbs of the internal capsule and also extending down to the corticospinal tracts (4). In previous reports, other findings were also observed including a low signal in the globus pallidus, substantia nigra, red nucleus (25, 27) and thalamus (28). Including these above-mentioned findings, the current ODDD patients presented with aberrant high signal findings in widespread areas from cerebral subcortical regions to brainstem (midbrain and pons). Roscoe et al (29) showed in the first functional study of two missense mutations, one in the first transmembrane (TM1) domain (p.G21R) and the other in the cytoplasmic loop (p.G138R), that the mutant proteins were able to reach cell-cell interfaces, but neither formed functional gap junction channels (30). In this study, the mutant proteins also interfered with the function of the wild-type protein. It is likely that the function of mutant Cx43-mediated gap junctions is reduced due to the dominant-negative effect on the wild-type protein.

The amino acid 25 of revelance in the present case is located in the TM1 domain, which is located in the cell membrane closed to the cytoplasm domain. In previous studies, missense mutations were observed in G21R, G22E and K23T (5, 8), which had each occurred sporadically. Although most ODDD cases are presented as autosomal dominant form, some cases of sporadic occurrence and recessive form are reported (13). In the present case, we could not examine DNA analysis because they did not permit the genetic test. According to this situation, this patient is considered to be a sporadic case. In sporadic cases, some alterations may allow complete gap junctions to form across cells, but their properties of conductance, molecular permeability, phosphorylation, and voltage gating are significantly altered, and cellular function is affected either as a dominant negative or a gain of function manner. In this regard, it is notable that five ODDD missense mutations (Y17S, S18P, G21R, G22E and K23T) as well as S27P are clustered within a region homologous to a calmodulin-binding motif of Cx32 (TM1) (31). Aberrant gating of gap junctions by calmodulin is thought to occur in response to changes in intracellular